Journal of Biomedical Optics

BiomedicalOptics.SPIEDigitalLibrary.org

Evaluation of fractional photothermolysis effect in a mouse model using nonlinear optical microscopy

Han Wen Guo
Te-Yu Tseng
Chen-Yuan Dong
Tsung-Hua Tsai

SPIE.

Evaluation of fractional photothermolysis effect in a mouse model using nonlinear optical microscopy

Han Wen Guo,[a] Te-Yu Tseng,[a] Chen-Yuan Dong,[a,b,c,*] and Tsung-Hua Tsai[d,*]
[a]National Taiwan University, Department of Physics, 1 Roosevelt Road, Section 4, Taipei 106, Taiwan
[b]National Taiwan University, Center for Quantum Science and Engineering, 1 Roosevelt Road, Section 4, Taipei 106, Taiwan
[c]National Taiwan University, Center for Optoelectronic Biomedicine of Medicine, 1 Roosevelt Road, Section 4, Taipei 106, Taiwan
[d]Cathay General Hospital, Department of Dermatology, 280 Renai Road, Section 4, Taipei 106, Taiwan

Abstract. Fractional photothermolysis (FP) induces discrete columns of photothermal damage in skin dermis, thereby promoting collagen regeneration. This technique has been widely used for treating wrinkles, sun damage, and scar. In this study, we evaluate the potential of multiphoton microscopy as a noninvasive imaging modality for the monitoring of skin rejuvenation following FP treatment. The dorsal skin of a nude mouse underwent FP treatment in order to induce microthermal zones (MTZs). We evaluated the effect of FP on skin remodeling at 7 and 14 days after treatment. Corresponding histology was performed for comparison. After 14 days of FP treatment at 10 mJ, the second harmonic generation signal recovered faster than the skin treated with 30 mJ, indicating a more rapid regeneration of dermal collagen at 10 mJ. Our results indicate that nonlinear optical microscopy is effective in detecting the damaged areas of MTZ and monitoring collagen regeneration following FP treatment. [DOI: 10.1117/1.JBO.19.7.075004]

Keywords: fractional photothermolysis; second harmonic generation; collagen regeneration; wound healing.

Paper 140292RR received May 9, 2014; revised manuscript received Jun. 11, 2014; accepted for publication Jun. 12, 2014; published online Jul. 14, 2014.

1 Introduction

Ablative skin resurfacing and nonablative dermal remodeling are currently accepted techniques for treating photoaged skin. Ablative skin resurfacing using CO_2 or Erbium:YAG laser can volatilize the skin tissue and cause photothermal damage to induce tissue coagulation.[1,2] The side effects and longer recovery time after ablative skin resurfacing are less desirable for many patients. On the other hand, nonablative dermal remodeling results in photothermal damage without volatilizing skin tissue, thereby minimizing the side effects of skin treatment.[3] To further improve the side effects and the recovery time, fractional photothermolysis (FP) was introduced to create discrete columns of photothermal damage to specific depths into the tissue. With the formation of heat shock proteins in the microthermal zones (MTZs), collagen regeneration in the skin dermis is promoted. In contrast to traditional treatment modalities, epidermal integrity is better preserved as each MTZ is surrounded by healthy tissue. As a result, healing is rapid as the recovery time dramatically reduced.[4,5]

The FP treatment can be used for the treatment of wrinkles, sun damage, and scars. The density, the depth, and the spot size of MTZs can be adjusted in order to target the intended tissue in a precise manner.[6] Adjustment of these parameters can considerably affect the outcome of the FP treatment. Until now, the status of the treated skin and treatment outcome are evaluated with biopsy, a gold standard in clinical medicine. However, this method is time-consuming, invasive, and may result in side effects such as surgical scar formation. Furthermore, information from treated skin cannot be immediately obtained and monitored so that the optimal time point of treatment may be delayed. Thus, noninvasive techniques are required in clinics for monitoring the parameters of MTZ and treatment outcome.

Recently, numerous noninvasive imaging technologies, such as optical coherence tomography (OCT),[7] confocal microscopy,[8] and second harmonic generation (SHG) microscopy,[9] have been developed to visualize the structures of skin tissue. Specifically, SHG microscopy is a useful technique for visualization of tissue structure as it holds several unique advantages, such as reduced specimen photodamage, higher contrast images, and enhanced penetration.[10,11] Recently, SHG became increasingly popular in the application of dermatology as this technique can be used to visualize collagen fiber in the dermis.[12] Specifically, SHG has been applied to monitor thermally induced structural transitions of collagen and to predict heat-induced collagen shrinkage.[13] Furthermore, the combination of multiphoton autofluorescence (MAF) and SHG imaging has been applied to visualize thermal damage in radiofrequency-irradiated skin.[14] Multiphoton microscopy (MPM) has also found applications in wound healing,[15] as the characterization of skin thermal damage in *ex vivo* human skin demonstrated.[16,17] These findings indicated that nonlinear optical microscopy can be used as an effective monitoring system for evaluating the effect of the FP treatment on the skin.

The outcome of the FP treatment depends largely on the parameters associated with MTZs. In this study, we performed FP with different energies on nude mouse skin. After FP treatment, morphologic changes of epidermis and dermis were imaged using SHG and MAF microscopy for 2 weeks. In addition, quantitative changes of the SHG signal were used to evaluate the outcome of the FP treatment. In this manner, we evaluated the potential of MPM in detecting the effect and subsequent outcome of the FP treatment.

*Address all correspondence to: Chen-Yuan Dong, E-mail: cydong@phys.ntu.edu.tw; Tsung-Hua Tsai, E-mail: tsaitsunghua@yahoo.com.tw

0091-3286/2014/$25.00 © 2014 SPIE

2 Materials and Methods

2.1 *Fractional Photothermolysis Treatment Procedures*

The shaved dorsal skin of nude mice (National Laboratory Animal Center, Taipei, Taiwan) was treated by FP through a 1550-nm erbium-doped fiber laser with a roller handpiece (Fraxel® laser SR 1500, Reliant Technologies, Palo Alto, California, USA). Exposures of 10 and 30 mJ, two illumination conditions, were performed (one pass) on mice to create MTZ densities of $326/cm^2$ and $108/cm^2$, respectively. These two energy settings were selected to study the recovery process in superficial dermis (10 mJ) and deeper dermis (30 mJ). In addition, we did not observe adverse side effects to the mice as the MTZs remained in the dermis. These two settings resulted in the same treatment level (coverage area). At Days 0, 7, and 14 following FP treatment, ~ 1 cm^2 of the skin specimen was excised from the dorsal region of each mouse and stored in 10% formalin solution (Sigma-Aldrich, St. Louis, Missouri) for imaging and histological examinations. The control samples were excised from the nude mouse without FP treatment.

2.2 *Multiphoton Autofluorescence and Second Harmonic Generation Imaging*

The MAF and the SHG images of skin were acquired through the use of a homemade multiphoton microscopic system as previously reported.[18] Briefly, skin samples were imaged with a multiphoton laser scanning microscope and with a PlanFlour $20\times$/NA 0.75, water-immersion objective lens (Nikon, Tokyo, Japan). The MAF and the SHG signal were excited at 780 nm by a diode solid-state laser-pumped mode-locked femtosecond Ti:sapphire laser (Tsunami; Spectra Physics, Mountain View, California, USA) and the emitted autofluorescence and the SHG signal were detected at the wavelength range of 470 to 635 nm and 380 to 400 nm, respectively. Emitted photons were detected by photomultiplier tubes (R7400P; Hamamatsu, Hamamatsu, Japan). Due to the unevenness of the skin's inherent structure, we determined the skin surface by first detecting the skin epithelium through the MAF imaging. The skin surface is then defined to be about 10 μm below the topmost layer of the imaged epithelium skin. The images were acquired at depths of approximately 0, 20, 40, 60, 80, and 100 μm from the surface of the skin. All acquired optical images were 228×228 μm^2 in area with a resolution of 256×256 pixels. To visualize skin samples on a large scale, a specimen translation stage (H101, Prior Scientific Instruments, Cambridge, United Kingdom) was used to translate the specimen after the acquisition of each small area of optical image. In all, 16 adjacent images (4×4) were acquired and assembled into a larger scale image (912×912 m^2).

2.3 *Image Processing and Analysis*

The MPM images were analyzed and reconstructed by use of ImageJ 1.47v (National Institutes of Health, Bethesda, Maryland, USA). This program allows visual inspection of

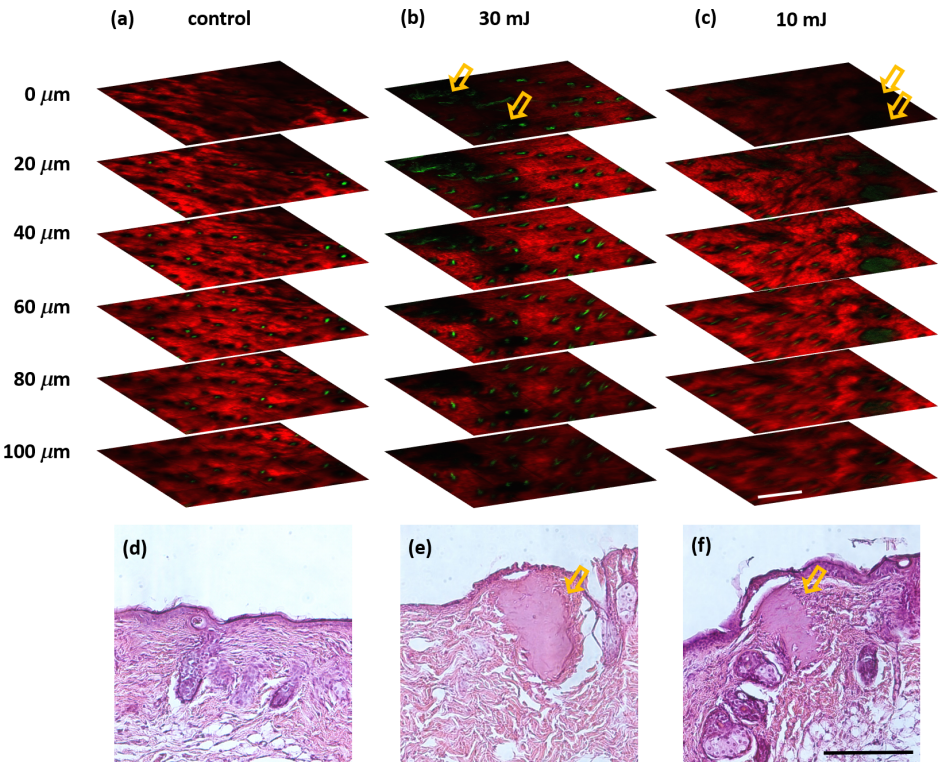

Fig. 1 *En face* second harmonic generation (SHG) (red) and multiphoton autofluorescence (MAF) (green) images of untreated (a) and fractional photothermolysis (FP)-treated nude mouse skin at 30 mJ (b) and 10 mJ (c) were acquired from the surface to the depth of 100 μm. Dark regions in (b) and (c), indicated by the yellow arrow, are locations of the microthermal zones (MTZs). The histological image (d) to (f) corresponded to SHG (red) and MAF (green) images of untreated and FP-treated nude mouse skin at 30 and 10 mJ, respectively. The yellow arrow indicated the MTZ location caused by FP treatment. The scale bar in (c) and (f) is 200 μm.

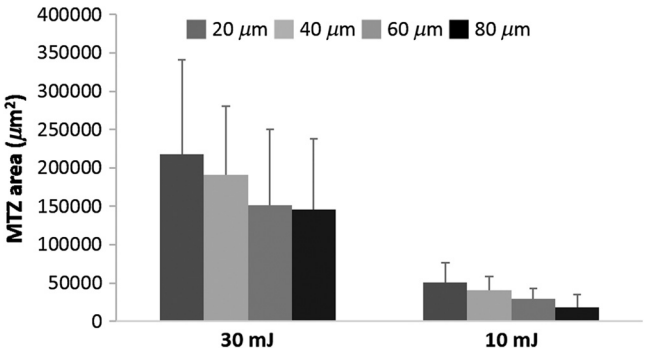

Fig. 2 MTZs areas from FP treatment at 30 and 10 mJ were estimated from *en face* SHG images at the depth of 20, 40, 60, and 80 μm.

various morphologic features and fluorescence patterns of cellular components within the skin specimens. The SHG signal of skin was determined by setting a threshold at each image to exclude the counts located at the lowest 5% SHG intensity. This value was selected since we found that the SHG signal from one frame is ~20 times that of the background. Therefore, we used 5% as the cutoff in analyzing the SHG intensity. In this manner, the SHG signal of each image was presented by the percentage of all pixel counts, which is indicative of the second harmonic generating collagen that is present. The data presented are determined from at least five independent images.

2.4 *Histological Examination*

Full-thickness dorsal skin was excised and prepared for comparable histological examination. The histological preparation includes specimen fixation in 10% buffered formaldehyde solution followed by dehydration using ethanol. Subsequently, the specimen was embedded in paraffin wax and stained with hematoxylin and eosin.

3 Results

3.1 *Fractional Photothermolysis Treatment-Induced Damage Revealed by Multiphoton Imaging*

To visualize the photothermal damage on mouse skin, we performed *ex vivo* SHG and MAF imaging immediately after the FP treatment at 10 and 30 mJ. As shown in Figs. 1(a)–1(c), these *en face* multiphoton images were acquired at intervals of 20-μm depth from the skin surface to a 100-μm depth. Compared to control images, the disappearance of the SHG signal in the multiphoton images as indicated by the yellow arrow, revealed FP treatment-induced damage on skin collagen. The larger damaged area and several smaller damaged areas were observed in

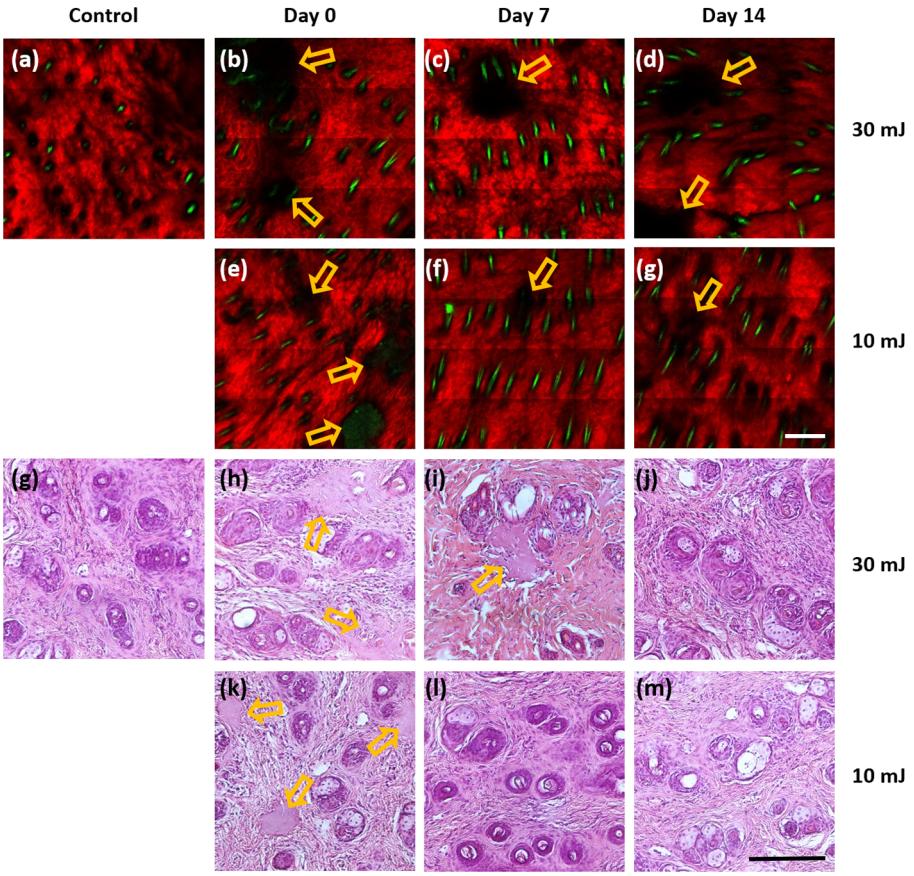

Fig. 3 *En face* SHG (red) and MAF (green) images of mouse skin were acquired at the depth of 40 μm: normal skin (a); treated skin at Days 0 (b), 7 (c), and 14 (d) post FP treatment at 30 mJ; treated skin at Days 0 (e), 7 (f), and 14 (g) post FP treatment at 10 mJ. Histological images corresponded to SHG (red) and MAF (green) images: normal skin (g); treated skin at Days 0 (h), 7 (i), and 14 (j) post FP treatment at 30 mJ; treated skin at Days 0 (k), 7 (l), and 14 (m) post FP treatment at 10 mJ. The yellow arrow indicates the location of MTZ. The scale bar in (g) and (m) is 200 μm each.

FP-treated specimens at 30 and 10 mJ, respectively, which correspond to the Fraxel® laser setup (108/cm^2 MTZs at 30 mJ and 326/cm^2 MTZs at 10 mJ). Localized melting and structural changes (i.e., MTZs) of mouse skin can be seen in the corresponding histological images [Figs. 1(d)–1(f)] following FP treatment, indicating that the disappearance of the SHG signal in the multiphoton images is due to FP treatment-induced collagen damage.

En face MPM images along the *z*-axis direction revealed the structures of MTZs at different depths. Moreover, the averaged areas of MTZs at various depths can be quantitatively evaluated from the *en face* results. The complete MTZs of five images were circled to estimate the damaged areas. Figure 2 show the averaged areas of MTZs at the depths of 20, 40, 60, 80 μm from the surface of the skin. We excluded the results at the depths of 0 and 100 μm due to the clear edges of MTZs at the skin surface and because the deeper depth are difficult to determine. The result showed a trend such that the area of MTZs decreases as the depth increases, which is most likely due to the decay of pulse energy with the increasing depth.

3.2 *Multiphoton Imaging of Skin Rejuvenation After Fractional Photothermolysis Treatment*

To evaluate skin rejuvenation after the FP treatment, *ex vivo* SHG and MAF images were acquired at Days 0, 7, and 14 post FP treatment. Figure 3(a) shows an *en face* MPM image at a depth of 40 μm at Days 0, 7, and 14 post FP treatment. The decrease in the area of MTZs with time was observed at both energies of 30 and 10 mJ, indicating collagen regeneration following FP treatment. Compared to the FP treatment of 30 mJ, the smaller area of MTZ was found 7 days following an FP treatment at 10 mJ. In the corresponding histological images [Fig. 3(b)], the large and the small MTZs are visible at Day 0 after FP treatment with 30 and 10 mJ. Similar to our MPM images, the MTZs became less significant with time [Fig. 3(b)]. At Days 7 and 14 after the FP treatment of 10 mJ, it is difficult to identify the FP modified regions from the histological images.

3.3 *Quantitative Second Harmonic Generation Analysis in Evaluating the Effect of Fractional Photothermolysis Treatment on Collagen Rejuvenation*

The SHG intensity of skin has been used as an index of collagen structural disruption and skin rejuvenation.[9,19,20] For quantitative SHG analysis, each of three mice underwent FP treatment at 30 and 10 mJ, then at least five *ex vivo* MPM images were acquired at every time point. The percentage of the SHG area in each image was determined to evaluate collagen rejuvenation. To investigate dermal rejuvenation, the percentage of the SHG area was analyzed on normal and FP-treated skin. In Fig. 4, results at the depths of 20 and 80 μm are shown. Since the thickness of mouse epidermis is around 20 μm,[21] the results at a depth of 20 μm would represent the physiological changes at the upper dermis, whereas that at a depth of 80 μm represents corresponding changes in the deeper dermis. The percentage of the SHG area of normal skin at the depths of 20 and 80 μm are 85 $\pm$ 3% and 81.8 $\pm$ 1.3% of all pixel counts, respectively. On Day 0 following FP treatment, the SHG signal at the depth of 20 μm decreased to 51.8 $\pm$ 9.8% (30 mJ) and 56.8 $\pm$ 2.6% (10 mJ). Subsequently, on Day 14, the percentage of the SHG area increased to 68 $\pm$ 2.8% (30 mJ) and 77.7 $\pm$ 5.1% (10 mJ). A similar trend was observed at the depth of 80 μm as the

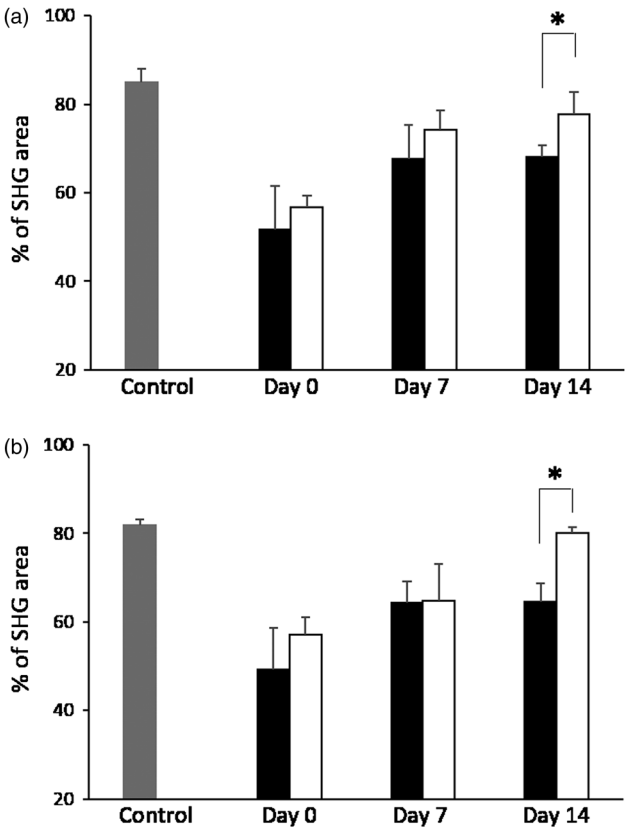

Fig. 4 Percentage of SHG area was quantitatively analyzed from *en face* SHG images at 20 μm (a) and 80 μm (b). The gray bar corresponds to the control result. The black and white bars are the results of 30 and 10 mJ, respectively. * indicates that significant difference exits ($p < 0.05$, *student's t-test*).

percentage of SHG area increased from 49.3 $\pm$ 9.3% to 64.6 $\pm$ 4.2% (30 mJ) and from 57.2 $\pm$ 3.8% to 80 $\pm$ 1.3% (10 mJ) on Day 14. These results indicated that the collagen regeneration occurred throughout the dermis and can be investigated by multiphoton imaging. Additionally, compared to the FP treatment at 30 mJ, the SHG signal recovered more quickly at 10 mJ.

4 Discussion

The FP treatment causes nonablative fractional dermal remodeling through collagen regeneration and has been reported in the treatment of wrinkles, sun damage, scars, and spider veins. The penetration depth and spot size of MTZ are important factors for this technique. In addition, multiple treatments are usually required in the clinics, and periods of treatments depend on the doctor's clinical experience. Therefore, noninvasive imaging techniques are required for monitoring the MTZ parameters and treatment outcomes. Recently, an OCT system was reported to visualize the structure of the skin and analyze the damaged area at various depths following ablative fractional skin resurfacing and nonablative fractional dermal remodeling.[7,22,23] A damaged skin structure showed changes in scattering properties such that the MTZs can be detected and analyzed. In comparison, the SHG signal is specific to fibrillar collagen remodeling in the dermis. Therefore, in evaluating collagen regeneration by the FP treatment, SHG microscopy is an appropriate technique. In this study, we used a mouse model to demonstrate that SHG microscopy is a useful tool for monitoring collagen regeneration post FP treatment. In the Fraxel laser setting, large but low-density

MTZs were induced by the FP treatment at 30 mJ. In contrast, the FP treatment at 10 mJ resulted in small and high density MTZs for the same coverage area (treatment level) setting. These two FP energy settings were used on the skin of nude mice.

To visualize MTZs through SHG imaging, *en face* SHG and MAF images from the surface of the skin to the depth of 100 μm were acquired. The *en face* SHG and MAF images along the z-axis direction clearly showed the presence of MTZs [Figs. 1(b) and 1(c)], as the spot size of MTZ decreased with increasing depth. The damaged area analysis also showed a decreasing trend from a depth of 20 to 80 μm (Fig. 2). The large deviation at each depth is due to the fact that the damaged area induced by FP treatment is influenced by parameters such as the incident angle of the optical beam and the optical properties of skin. Additionally, damaged areas of MTZ induced by the FP treatment were analyzed through histological examination [Figs. 1(e) and 1(f)]. These results demonstrated that SHG microscopy can be effectively used to visualize the MTZs.

To evaluate skin rejuvenation after the FP treatment, *en face* SHG and MAF images were acquired at Days 0, 7, and 14 following FP treatment. The SHG images showed that the damaged area decreased at Days 7 and 14 after the FP treatment at 30 and 10 mJ (Fig. 3). Quantitative SHG analysis also showed an increasing trend at both of the depths (Fig. 4). On the other hand, differing from the SHG images, disruption in collagen structure is difficult to identify from the surrounding reticular dermis in the histological images (Day 7). Compared to a histological examination, the SHG signal is effective for investigating collagen regeneration due to its specificity to collagen fiber. In addition, quantitative SHG analysis showed that the dermal collagen recovered faster under the FP treatment of 10 mJ than at 30 mJ (Fig. 4). This finding suggested that the smaller but high density MTZs can induce collagen regeneration faster in our nude mouse model.

By use of an *ex vivo* mouse model, we demonstrated that SHG microscopy is capable of detecting the parameters of the induced MTZ and monitoring collagen regeneration after FP treatment. In this study, we successfully visualized the damaged area of MTZ at various depths by SHG and MAF imaging. By the subsequent analysis of SHG signal on mouse skin, collagen regeneration after the FP treatment can be evaluated. In addition, a different MTZ-damaged area and a different recovery of collagen regeneration from the FP treatment can be resolved from the two different energies. Our study suggested that SHG microscopy can be further developed into a real-time, feedback system for evaluating responses to FP treatment *in vivo*.

Acknowledgments

This work was supported by grants from the National Science Council of Taiwan (NSC102-2221-E-002-030-MY3, NSC100-2314-B-418-009-, and NSC101-2112-M-002-003-MY3), National Health Research Institutes (NHRI-EX102-10041EI), National Taiwan University (NTU-102R7804 and CQSE-102R891401), and a project of "Aim for Top University Plan" sponsored by the Ministry of Education, Executive Yuan, Taiwan.

References

1. T. S. Alster and S. Garg, "Treatment of facial rhytides with a high-energy pulsed carbon dioxide laser," *Plast. Reconstr. Surg.* **98**(5), 791–794 (1996).
2. C. B. Zachary, "Modulating the Er:YAG laser," *Lasers Surg. Med.* **26**(2), 223–226 (2000).
3. E. V. Ross et al., "Nonablative skin remodeling: selective dermal heating with a mid-infrared laser and contact cooling combination," *Lasers Surg. Med.* **26**(2), 186–195 (2000).
4. D. Manstein et al., "Fractional photothermolysis: a new concept for cutaneous remodeling using microscopic patterns of thermal injury," *Lasers Surg. Med.* **34**(5), 426–438 (2004).
5. M. Wanner, E. L. Tanzi, and T. S. Alster, "Fractional photothermolysis: treatment of facial and nonfacial cutaneous photodamage with a 1,550-nm erbium-doped fiber laser," *Dermatol. Surg.* **33**(1), 23–28 (2007).
6. T. Kono et al., "Prospective direct comparison study of fractional resurfacing using different fluences and densities for skin rejuvenation in Asians," *Lasers Surg. Med.* **39**(4), 311–314 (2007).
7. M. T. Tsai et al., "Noninvasive characterization of fractional photothermolysis induced by ablative and non-ablative lasers with optical coherence tomography," *Laser Phys.* **23**(7), 075604 (2013).
8. V. Czaika et al., "Application of laser scan microscopy *in vivo* for wound healing characterization," *Laser Phys. Lett.* **7**(9), 685–692 (2010).
9. S. J. Lin et al., "Prediction of heat-induced collagen shrinkage by use of second harmonic generation microscopy," *J. Biomed. Opt.* **11**(3), 034020 (2006).
10. S. J. Lin, S. H. Jee, and C. Y. Dong, "Multiphoton microscopy: a new paradigm in dermatological imaging," *Eur. J. Dermatol.* **17**(5), 361–366 (2007).
11. P. T. C. So et al., "Two-photon excitation fluorescence microscopy," *Ann. Rev. Biomed. Eng.* **2**(1), 399–429 (2000).
12. K. Konig and I. Riemann, "High-resolution multiphoton tomography of human skin with subcellular spatial resolution and picosecond time resolution," *J. Biomed. Opt.* **8**(3), 432–439 (2003).
13. S. J. Lin et al., "Monitoring the thermally induced structural transitions of collagen by use of second-harmonic generation microscopy," *Opt. Lett.* **30**(6), 622–624 (2005).
14. T.-H. Tsai et al., "Visualizing radiofrequency–skin interaction using multiphoton microscopy *in vivo*," *J. Dermatol. Sci.* **65**(2), 95–101 (2012).
15. A. T. Yeh et al., "Imaging wound healing using optical coherence tomography and multiphoton microscopy in an *in vitro* skin-equivalent tissue model," *J. Biomed. Opt.* **9**(2), 248–253 (2004).
16. B. R. Masters et al., "Mitigating thermal mechanical damage potential during two-photon dermal imaging," *J. Biomed. Opt.* **9**(6), 1265–1270 (2004).
17. M. G. Lin et al., "Evaluation of dermal thermal damage by multiphoton autofluorescence and second-harmonic-generation microscopy," *J. Biomed. Opt.* **11**(6), 064006 (2006).
18. T.-Y. Tseng et al., "Investigation of transport dynamics in oleic acid–induced transdermal drug delivery by two-photon fluorescence microscopy: an ex-vivo study of mouse skin," *J. Biomed. Opt.* **18**(9), 096016 (2013).
19. A. T. Yeh et al., "Reversible dissociation of collagen in tissues," *J. Invest. Dermatol.* **121**(6), 1332–1335 (2003).
20. Y. Sun et al., "Investigating mechanisms of collagen thermal denaturation by high resolution second-harmonic generation imaging," *Biophys. J.* **91**(7), 2620–2625 (2006).
21. K. Calabro et al., "Gender variations in the optical properties of skin in murine animal models," *J. Biomed. Opt.* **16**(1), 011008 (2011).
22. G. B. Altshuler et al., "Methods and devices for fractional ablation of tissue for substance delivery," Google Patents (2009).
23. E. A. Genina et al., "Transcutaneous delivery of micro- and nanoparticles with laser microporation," *J. Biomed. Opt.* **18**(11), 111406 (2013).

Biographies of the authors are not available.